

Potential-Dependent Chloride Threshold in Reinforced Concrete Damage Prediction – Effect of Activation Zone Size

Andrea N. Sánchez and Alberto A. Sagüés
University of South Florida
Department of Civil and Environmental Engineering
4202 East Fowler Ave.
Tampa, FL 33620 U.S.A.

ABSTRACT

Previous work has shown that chloride corrosion threshold increases when steel bar potentials are more cathodic than -200 ± 50 mV (SCE). When corrosion starts at a given location, the steel of the adjacent regions remains in its passive state; therefore corrosion initiation is delayed in those regions due to the negative shift in potential. Introduction of threshold dependence on potential is a critical need for accurate forecasting, as neglecting that phenomenon can lead to erroneously high damage projections. An earlier investigation incorporated this issue in a one-dimensional deterministic model solved by a finite difference method evaluating a partially submerged reinforced concrete column. While the model served to demonstrate feasibility of the concept, damage prediction was found to be highly sensitive to the corrosion activation zone size. As the number of nodes used for the model increased, resulting in smaller activation zones, the total predicted amount of damage at a given age decreased. Examination of the model assumptions suggested that the problem stemmed from neglecting the local resistance of the concrete around the steel bars. An improvement has been developed here by implementing a formulation that accounts for the local resistance polarization associated with the selection of the size of activation zone. The damage projections for the smaller node separation resulted in a finite limiting value. Comparison with a case where the effect of local resistance polarization in the activation zone size is neglected is presented.

Key words: chloride corrosion threshold, modeling, steel potential, corrosion, concrete, active zone size, resistance polarization.

INTRODUCTION

Corrosion of steel in concrete initiates once the concentration of chloride ions at the steel surface reaches a minimum required amount, defined as the chloride corrosion threshold, C_T .

Corrosion forecasting models largely follow Tuutti's initiation-propagation stages concept.¹ There the

©2013 by NACE International.

Requests for permission to publish this manuscript in any form, in part or in whole, must be in writing to NACE International, Publications Division, 1440 South Creek Drive, Houston, Texas 77084.

The material presented and the views expressed in this paper are solely those of the author(s) and are not necessarily endorsed by the Association.

value of C_T plays a key role in commonly used approaches to estimate the length of the initiation stage, along with the chloride surface concentration (C_S), chloride diffusion coefficient (D), and concrete cover (X_C). While the value of C_T is assigned a random range of variability in some model implementations, C_T is commonly assumed to be time invariant and not affected by the corrosion state of nearby portions of the rebar assembly.²

There is increasing evidence that the chloride corrosion threshold increases when the still passive steel is polarized to potential values more cathodic than the typical open circuit potential in atmospherically exposed concrete. The latter is in the order of ~ -100 mV versus saturated calomel electrode (SCE; all potentials in the following will be reported in this scale).³ An updated version of a literature review by Presuel et al on the relationship between C_T and steel potential (E) is shown in Figure 1.^{2,4} Despite the scatter, it can be seen that at potentials $> \sim -100$ mV the values of C_T are roughly independent of E , but that at more negative potentials the values of C_T tend to follow an exponential increase with additional cathodic polarization. A recent investigation by Sánchez and Sagüés [2] (gray diamonds in Figure 1) provided further support of that threshold dependence on potential (TDP) trend. An envelope trend line, such as that drawn in Figure 1, may be described in general terms by Equation (1):

$$\log_{10} \left(\frac{C_T}{C_{T0}} \right) \sim \frac{E_{T0} - E}{\beta_{CT}} \quad (1)$$

where C_T is the threshold expressed as percentage of cement content in the concrete, E is the potential of the steel bar, while still in the passive condition, β_{CT} is the characteristic inverse slope of the increase of C_T in a E - $\log C_T$ representation and E_{T0} and C_{T0} are constants. This effect is the basis of the cathodic prevention method, whereby reinforcing steel is cathodically polarized while still in the passive condition to delay or prevent corrosion due to the elevation of the corrosion threshold.^{5,6}

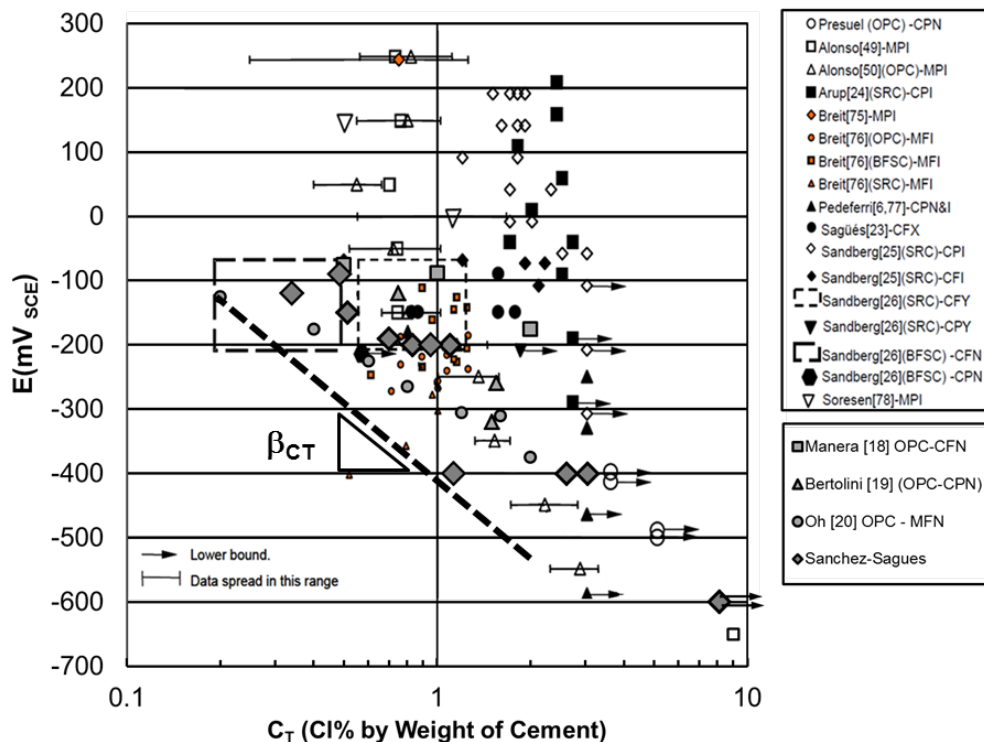


Figure 1. Chloride threshold dependence on steel potential compilation by Presuel, updated by Sánchez.^{4,2} Notation: OPC: Ordinary Portland Cement; SRC: Sulfate resistant cement; BFSC: Blast furnace slag cement; M: mortar or C: concrete; P: Polarized or F: open circuit potential; I: Immersed or N: Not Immersed; X: cyclic or permanent ponding; Y: splash zone or Z: simulated splash zone). Dashed line: see text.

©2013 by NACE International.

Requests for permission to publish this manuscript in any form, in part or in whole, must be in writing to NACE International, Publications Division, 1440 South Creek Drive, Houston, Texas 77084.

The material presented and the views expressed in this paper are solely those of the author(s) and are not necessarily endorsed by the Association.

The redundant 3-parameter line formulation is chosen for convenience to match the form of other ruling equations in electrochemical systems.⁷ The dashed trend line shown in Figure 1 corresponds to values of $E_{TO} = -0.128$ V, $C_{T0} = 0.2$ % and $\beta_{CT} = -0.4$ V. Those parameter values, which represent a conservative lower envelope of the data⁽¹⁾ had been used in preceding TDP modeling simulations and were adopted for consistency in the present work as well. That choice is however not limiting and other parameter selections, presented elsewhere, may be more representative for engineering forecasting purposes.^{2,8-10}

Introduction of TDP is important for accurate corrosion forecasting, as neglecting that phenomenon can lead to erroneously high damage projections. This was shown in the previous work that incorporated TDP in a finite difference deterministic model of a partially submerged reinforced concrete column.⁸ The column was divided into zones of equal size. A surface chloride concentration pattern was assumed, as well as diffusional transport of chlorides into the concrete. Initially the steel potential was nearly uniform corresponding to a passive steel condition, which resulted in a threshold value that was nearly the same everywhere.

Corrosion started when the chloride corrosion threshold was first reached at the zone having the highest surface chloride content. That event resulted in activation of that zone and the creation of a macrocell corrosion pattern where that zone was anodic while the rest of the steel in the column remained as a passive, cathodic zone. The corrosion macrocell pattern for that configuration was then calculated to obtain the value of the steel potential E at every zone in the system. The still passive zones near that first activated developed a significantly more negative value of E than the one present before the first activation event. Hence, those zones were assigned per Eq. (1) a correspondingly larger value of C_T than before. Corrosion initiation in those regions was consequently delayed. As the newly calculated threshold value was eventually reached in other zones, the macrocell pattern was affected accordingly and corrosion development delayed in nearby regions as well. The overall result is a slower progression of corrosion in the system than if the threshold would have been a constant, potential-independent value. The effect, illustrated in Figure 2, was found to be a dramatic decrease in the predicted amount of corrosion damage when β_{CT} was finite (TDP) compared to the case of a potential-independent threshold ($\beta_{CT} = \infty$).

While those initial calculations served to reveal the importance of introducing TDP, that early model implementation had shortcomings that needed further resolution. In particular, it was noted that damage prediction was highly sensitive to the corrosion activation zone size.⁸ It was found that as the number of nodes used for the model increased, resulting in smaller activation zones, the total projected amount of damage at a given age decreased toward a zero limit value when node spacing was zero. That trend was clearly erroneous and constituted a major limitation in including TDP in damage projections.

Examination of the model assumptions suggested that the problem stemmed from neglecting the local resistance of the concrete around the steel bars. As a result, the macrocell coupling effect was inappropriately exaggerated as node spacing decreased leading to an erroneous limit condition. This paper presents a successful resolution of that issue by implementing an improved formulation that accounts for the local resistance polarization consistent with the size of activation zone.

⁽¹⁾ For example with a concrete with cement factor $C_F = 355$ Kg/m³ (600 pcy) the resulting value of C_T at E_{TO} , near typical open circuit potentials, is 0.71 Kg/m³ (1.2 pcy), which is an often adopted conservative threshold value.

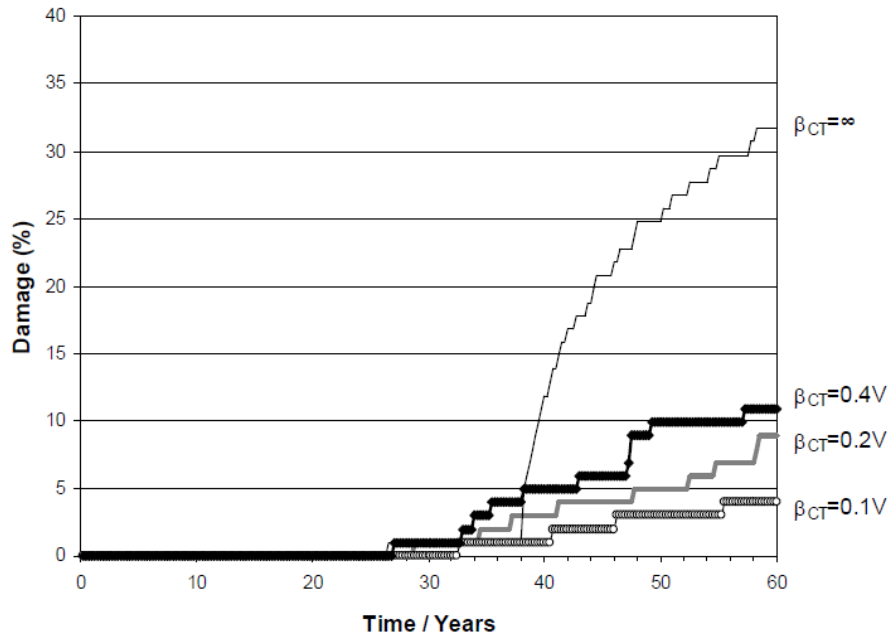


Figure 2. Damage projections in previous model calculations showing strong decrease in projected damage at age=60 years when comparing the case of a potential independent threshold ($\beta_{CT} = \infty$) and cases where C_T depended on potential of the passive steel. [8].

SYSTEM DETAILS

An illustration of the system modeled in the improved formulation is shown in Figure 3. It consists of a cylindrical reinforced concrete structure exposed to a marine environment and submerged to half its length L . It has a diameter ϕ , concrete cover X_C where the rebar mat is located. The following system description is identical to the one discussed in Reference⁹.

The system chosen for representation is a marine substructure, solid cylindrical reinforced concrete column partly submerged in seawater, of dimensions equivalent to those used when first introducing the potential-dependent threshold model.¹⁰ For simplicity, an idealized one-dimensional model was used here to represent the column, comparable to that employed by the authors in related work.¹¹ As shown there, that approach captures most of the features of interest of the system with minimum computational burden. The rebar mat, treated as a uniform sheet, has a total surface area of steel exposed to concrete equal to the external lateral column surface area multiplied by a Steel Factor S_F . The ends of the cylindrical column are considered to be isolated electrically and from the surrounding environment, and with no reinforcement.

The column is assumed to be immersed in seawater to half its length. The concrete is approximated as an effectively homogeneous electrolytic medium of resistivity ρ , effective chloride ion diffusivity D , and effective oxygen diffusivity D_O all of which are functions of elevation. Concrete on the lateral surface of the column is assumed to have developed very early a time-invariant chloride ion concentration C_S that is a function of elevation, and a time-invariant effective oxygen concentration C_{SO} treated as being constant with elevation.

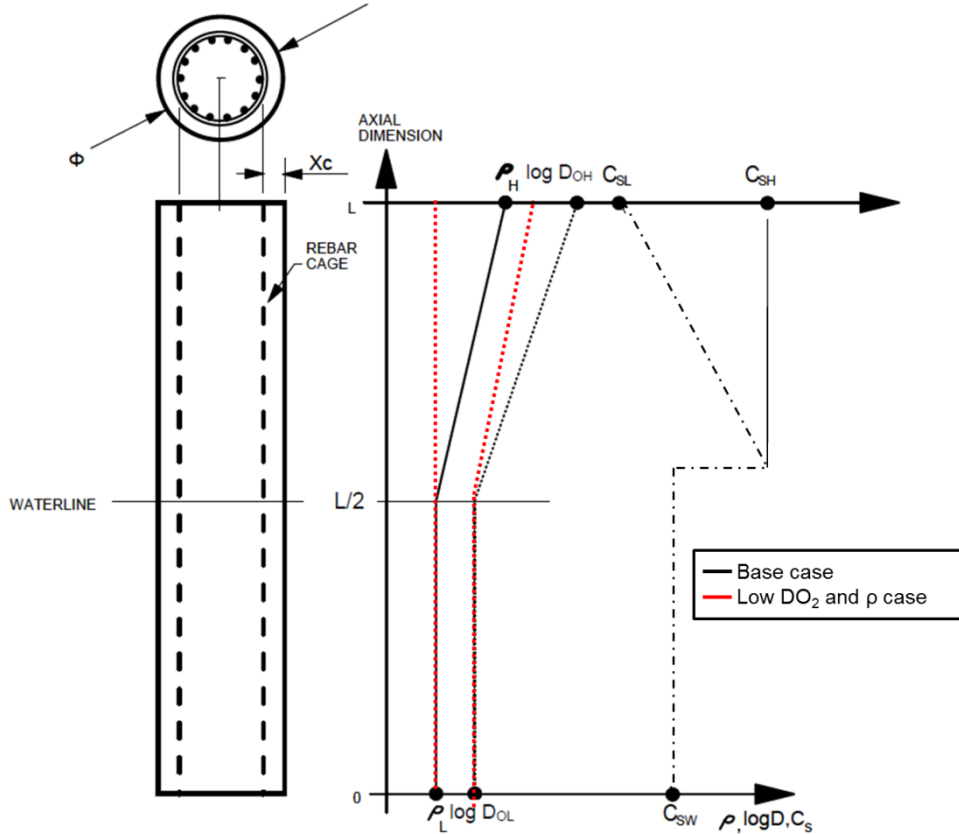


Figure 3. System modeled. Cases evaluated in this work. Dashed lines discusses in cases examined.

The reinforcing steel is assumed to be the locus of an anodic metal loss reaction as shown in Equation (3)



with a corresponding current density i_a , under two modalities: passive dissolution at a fixed small current density i_p , or active dissolution at a potential-dependent current density i_{aa} so that Equation (3a)

$$i_a = i_p \text{ (passive state)} \quad (3a)$$

And Equation (3b):

$$i_a = i_{aa} = i_{oa} 10^{\left(\frac{E-E_{oa}}{\beta a}\right)} \text{ (active state)} \quad (3b)$$

where i_{oa} is the nominal exchange current density, E_{oa} is the nominal equilibrium potential and βa is the anodic Tafel slope. The steel is also assumed to support a single cathodic reaction, oxygen reduction, Equation (4):



which is considered for simplicity to occur under either a fully activation-controlled or a fully diffusion-limited conditions. Under full activation control the current density is

$$i_{ca} = i_c = i_{oc} 10^{\left(\frac{E_{oc}-E}{\beta c}\right)} \quad (5)$$

where i_{oc} is the nominal exchange current density, E_{oc} is the nominal equilibrium potential and βc is the cathodic Tafel slope. Under full diffusional control the current density is Equation (6):

$$i_{cd} = i_c = \frac{4FDC_{SO}D_o}{X_c S_F} \quad (6)$$

where 4 is the number of electrons to reduce O_2 , $F = 96.5 \cdot 10^3$ coul/equiv is Faraday's constant, C_{SO} is the oxygen concentration in the pore water at the external concrete surface, and D_o is the effective diffusion coefficient of O_2 in the concrete, scaled to match the concentration units used. The value of i_c is made to switch from i_{ca} to i_{cd} when the former exceeds the latter, creating a working approximation in lieu of the more computationally mixed polarization function.¹²

As indicated in previous papers, the model computes the accumulation of chloride at the steel surface with time and declares elements active as the local value of C_T is exceeded.^{8,9} The corrosion propagation stage is addressed by computing the increasing amount of steel loss and declaring a given segment as damaged when a critical corrosion penetration amount is exceeded. Those features of the model are addressed in detail in the previous publications and will not be further treated here. In more detail the following concerns the computation of corrosion current distribution and potentials in the system, which is relevant to the new features introduced here.

Calling x the distance along the column axis, defining and treating the problem as one-dimensional in a manner similar to that used in Reference¹¹ the charge conservation condition implies that Equation (7):

$$i_s = \left(\frac{\emptyset}{4 S_F}\right) \left(\frac{1}{\rho} \frac{d^2 E}{dx^2} + \frac{d\rho^{-1}}{dx} \frac{dE}{dx}\right) \quad (7)$$

where $i_s = i_a - i_c$ is the net current density on the steel surface at elevation x , with i_a being equal to i_{aa} or i_p depending on whether the local steel surface was declared active or passive respectively if the value of C was respectively above or below the value of C_T .

Solution of Eq. (7) to obtain i_s and E as function of x is conducted iteratively for each time t using finite differences on a 101-node equispaced array along the elevation direction. The declaration of whether a given node corresponds to active or passive steel is made using the value of chloride concentration predicted by solution of Fick's 2nd law (as indicated in the previous papers [8,9]), and the local value of C_T calculated at each node per Eq.(1) using the value of E obtained at the end of the iterations conducted in the previous time step. The array of values of C_T remains unchanged during the iteration process. After iteration is complete the potential array is used as seed for the next time step potential calculations. It is noted that once steel at a given node is declared active, it remains so for all subsequent time steps. This is only a simplifying assumption that may be refined in future implementations of the modeling concept.

Equation (7) results from considering that the net current of the steel present in a length dx of column is equal to the difference in longitudinal current at each end of the element, as in a transmission line calculation. The respective current densities are inversely proportional to the lateral active surface of the element $S_F \pi \Phi dx$, and the cross sectional area of the element $S_F \pi \Phi^2 / 4$; the factors combine as shown when expressed in differential form. The longitudinal current density is proportional to the local longitudinal electric field. The formulation can be expressed equivalently in discretized electric circuit form as shown in Figure 4 following the treatment by Presuel, with segmental longitudinal resistance R_L

(Equation 8) and interfacial terms E_{si} related to i_{si} by the polarization equations given above and illustrated in Figure 5.¹¹

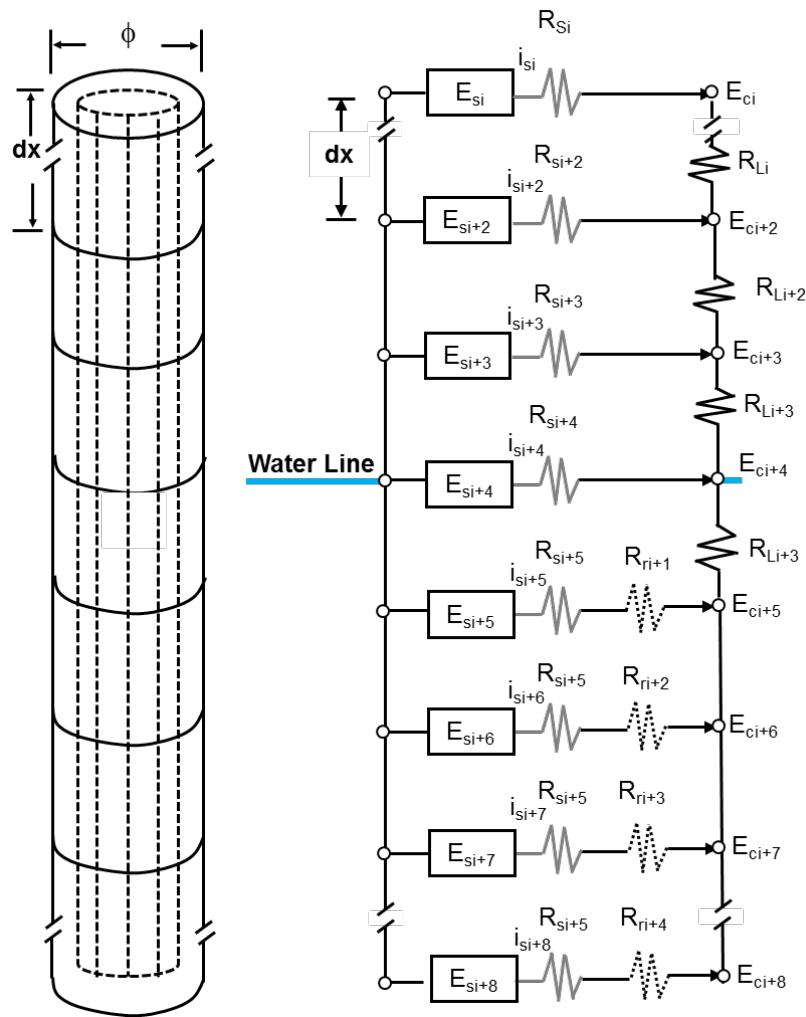


Figure 4. System discretization and types resistances used in the system showing a portion of the column near the waterline, starting at node i . Black resistor: longitudinal resistance. Dashed resistor: radial resistance. Gray resistor: steel resistance.

$$R_L = \frac{\Delta X \rho}{\left(\pi \frac{\phi^2}{4}\right)} \quad (8)$$

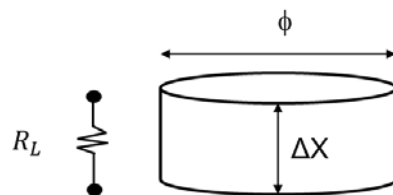


Figure 5. Longitudinal resistance for a segment ΔX)

where ΔX is the distance along the column axis, ρ is the local value of the concrete resistivity, ϕ is the diameter of the column.

In the simplified treatments given in previous versions of the model in References^{8,10} E_{si} for the above-water nodes was the same as the potential in the concrete in the same node, effectively assuming that there was no substantial potential drop between the rebar surface and the concrete nearby. Thus, any local resistance associated with geometric current constriction around the steel was considered negligible so the current density on the rebar surface was subject only to activation and concentration polarization (of the cathodic reaction only) of the reactions involved. For anodic segments providing cathodic prevention to surrounding passive regions, the activation-only limited anodic reaction was dominant, and it was unencumbered by the presence of a resistive term. Given the kinetic parameter choices used i , the resulting prevention effect extended over a relatively large region even if the active zone associated with a node was very small. In the below water segments a radial resistance factor was included called R_r , but only as a global factor that again did not sufficiently capture any local current concentration effect. That shortage was addressed here; by introducing a local resistance term R_S that was evaluated as follows.

The rebar was treated as a narrow cylindrical electrode of radius $\phi_r/2$ in a cylindrical medium that extended to an influence radius r_{iz} that is roughly approximated as $1/2$ of ϕ (Figure 6) as shown in Equation (9):

$$r_{iz} = \frac{1}{2}\phi \tag{9}$$

Using the equation for the resistance between concentric cylinders¹³, the current concentration resistance per unit length of rebar R_{SUL} is given by Equation (10):

$$R_{SUL} = \frac{\rho}{2\pi} \ln\left(\frac{r_{iz}}{\phi_r}\right) \tag{10}$$

Accounting for the length of rebar associated with S_F and the column dimensions, the amount of resistance R_S for each segment due to current concentration around the rebar is given by Equation (11)

$$R_S = \frac{R_{UL}\phi_r}{S_F\phi\Delta X} \tag{11}$$

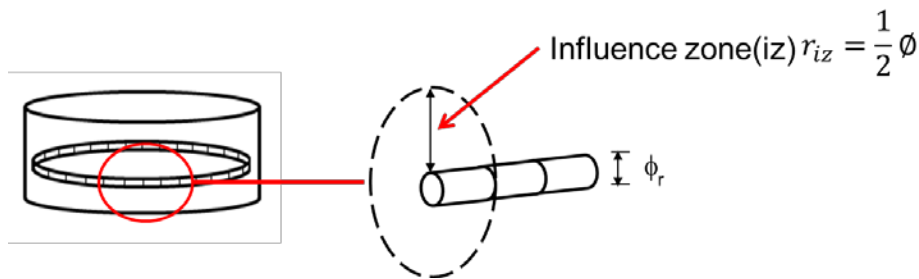


Figure 6. Local steel resistance (R_S) for a segment ΔX .

Introduction of R_S requires accounting for the potential difference between the immediate steel surface and the bulk of the surrounding concrete. In the previous model in Reference⁸ the term E described indistinctly the potential next to the steel surface and that in the bulk of the concrete. In the present treatment those are named E_s and E_c respectively and related to each other as shown in Eq.(12) and Fig.7 due to the presence of local resistance. E_s , the steel potential with respect to an ideal reference

electrode placed immediately next to the steel, rules the rate of the electrochemical reactions and hence needs to be used instead of E in Eqs. 3b and 5.

$$E_s = E - i_s R_s \quad (12)$$

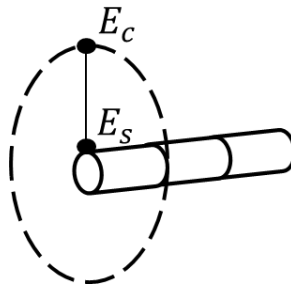


Figure 7. Relationship between E_c and E_s

Likewise, E_c rules the ohmic interaction between column segments and needs to be used instead of E in Eq. (8). The computation scheme was adjusted accordingly by making the necessary link between both potentials through Eq. 16. Introduction of R_s in the model captured a key element in providing a more realistic representation of the system, and in allowing simulations to converge toward a stable limit as the segment size was decreased. As implied by Eq. (14), a decreased segment size (equivalent to decreasing the size of the activation zone) increases the value of R_s and hence the relative extent of resistance polarization of the segment reactions.

ACTIVE ZONE SIZE

The expected relationship between activation zone and corresponding throwing power of the cathodic prevention effect can be further illustrated by the idealization shown in Figure 8. Here a portion of an individual rebar is addressed for clarity instead of the rebar in an entire column segment, but the overall concept applies in both cases.

A steel bar (initially in the passive state) is embedded in concrete with fixed C_T and E_s is represented in Figure 8 (a). Figure 8 (b and c) shows that after some time chloride ions coming non-uniformly from the exterior (1) caused C_T to be exceeded in a small zone where the passive film on the steel breaks down. A corrosion macrocell is formed with drop of E_s towards more negative values (3) around the active zone. The steel surrounding the active zone is still protected by the passive film, but due to macrocell coupling E in these regions (4) has a significantly lower value compared to the rest of the passive steel. Therefore C_T increases in these regions (per Eq.(1)) delaying corrosion initiation there. Figure 8 (c) illustrates a similar situation, but there the size of the activation zone was larger than that in 8b, and the size of the surrounding region where the increase in C_T is substantial is correspondingly larger as well. The influence zone is smaller with smaller activation zones because the macrocell effect is ohmically limited by local current constriction around a small anode.¹⁴ As activation zones become smaller, the corrosion preventing effect becomes smaller as well, and while the amount of corrosion per event is smaller, the number of events is expected to increase so a limiting condition is anticipated where the lower degree of corrosion mitigation is matched by the larger number of corroding spots.

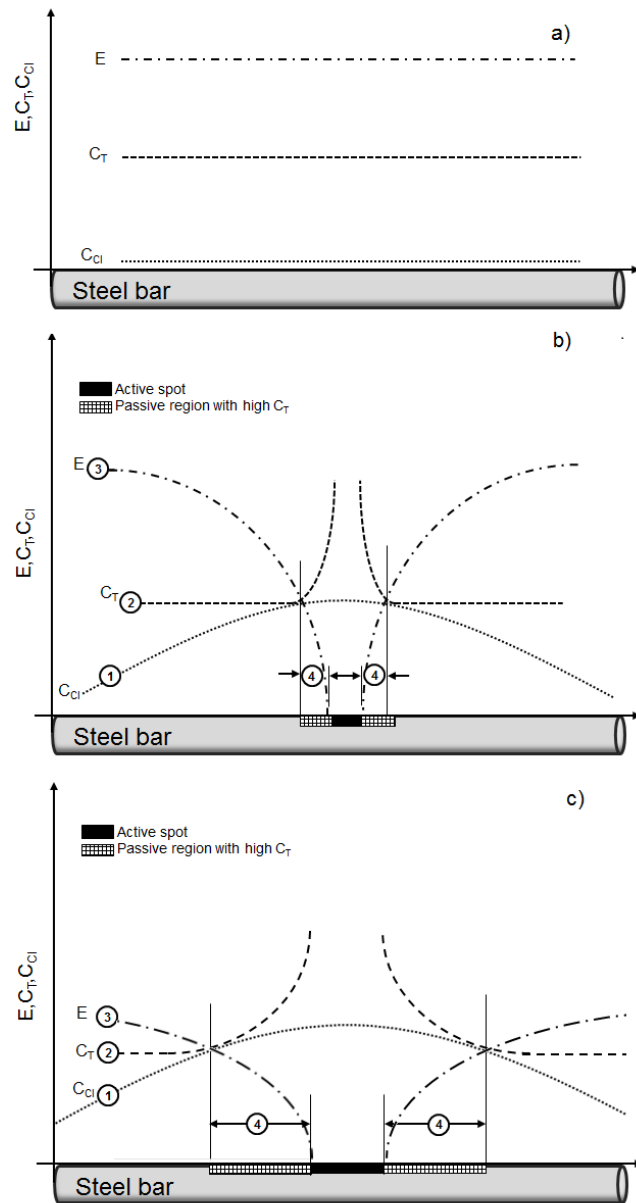


Figure 8. Passive and active state of a steel bar embedded in concrete considering the size of the activation spot. a) System at a passive state, b) system at an active state with small active spot, c) system at an active state with large active spot.

CASES EXAMINED

Base Case-NR corresponds to the input parameters evaluated in the so called “base case” in the previous model calculations [8] addressing resistance R_L only. Base Case-R is similar to Base Case-NR but incorporates the resistance R_S introduced here to address the activation zone size dependence noted above. Two other cases, Low DO_2 and ρ -NR and Low DO_2 and ρ -R are as in each of the above cases respectively, but in each the system has lower concrete resistivity and lower oxygen diffusivity. A summary of the model parameters are given in Table 1. The threshold dependence on potential in all these cases is assumed to correspond to a value of $\beta_{CT} = 0.4$ V.

As explained in a previous Reference⁸ lower resistivity and lower oxygen diffusivity are both expected to lead to a greater corrosion macrocell influence zone. Hence in these cases the effect of introducing TDP is expected to be stronger. These added cases offer a wider range of conditions in

©2013 by NACE International.

Requests for permission to publish this manuscript in any form, in part or in whole, must be in writing to NACE International, Publications Division, 1440 South Creek Drive, Houston, Texas 77084.

The material presented and the views expressed in this paper are solely those of the author(s) and are not necessarily endorsed by the Association.

which to evaluate to which extent introduction of R_s in the calculations acts to stabilize the limit response to activation zone decrease.

All cases were simulated by conducting calculations that included active zones equal to $\frac{1}{2}$, $\frac{1}{4}$ and $\frac{1}{8}$ times less than the steel element surface area of the “Base Case” from the previous model implementation in References⁸ which was done with a 101 node array. Those calculations were therefore made with numbers of nodes ranging from 101 to 801.

Table 1. Model parameters

MODEL PARAMETERS			
Steel Cover	$X_c = 10.5 \text{ cm}$		
Column diameter	$\Phi = 105 \text{ cm}$		
Column Length	$L = 1200 \text{ cm}$		
Cement factor	$C_F = 355 \text{ Kg/m}^3$		
Concrete Resistivity (Base Case)	$\rho_H = 2 \cdot 10^5 \text{ ohm-cm}$ $\rho_L = 4 \cdot 10^4 \text{ ohm-cm}$		
Concrete Resistivity (Low)	$\rho_H = 4 \cdot 10^4 \text{ ohm-cm}$ $\rho_L = 4 \cdot 10^4 \text{ ohm-cm}$		
Oxygen Diffusivity (Base Case)	$D_{OH} = 10^{-3} \text{ cm}^2/\text{sec}$ $D_{OL} = 10^{-5} \text{ cm}^2/\text{sec}$		
Oxygen Diffusivity (Low)	$D_{OH} = 10^{-4} \text{ cm}^2/\text{sec}$ $D_{OL} = 10^{-5} \text{ cm}^2/\text{sec}$		
Chloride Diffusivity	$D = 2 \cdot 10^{-8} \text{ cm}^2/\text{sec}$		
O ₂ Surface Concentration	$C_{SO} = 2.5 \cdot 10^{-7} \text{ mol/cm}^3$		
Cl ⁻ Surface Concentration	$C_{SH} = 15 \text{ Kg/m}^3$ $C_{SW} = 9 \text{ Kg/m}^3$ $C_{SL} = 0 \text{ Kg/m}^3$		
Chloride Threshold Parameters	$C_{TOS} = 0.71 \text{ Kg/m}^3$ $E_{TO} = -128 \text{ mV}$ $\beta_{CT} = 400 \text{ mV}$		
Polarization Parameters	E_0 (-mV CSE)	i_0 (A/cm ²)	Tafel Slope (mV)
Iron Dissolution	-780	$1.875 \cdot 10^{-8}$	60
Oxygen Reduction	+160	$6.25 \cdot 10^{-10}$	160
Steel Passive			
Current Density	$i_p = 0.058 \cdot 10^{-6} \text{ A/cm}^2$		
Critical Corrosion Penetration	$P_{CRIT} = 0.01 \text{ cm}$		
Active Zone Size	Corresponding to 1 node (Base) Corresponding to $\frac{1}{2}$, $\frac{1}{4}$ and $\frac{1}{8}$ base case node		

RESULTS AND DISCUSSION

Figure 9 compares the damage projection values, expressed as percentage of the column surface affected by corrosion spalls, for 60 years of service life for calculations that incorporate the effect of R_s (open symbols), and those not incorporating it as the previous modeling approach (solid symbols).⁸ The results are given as function of the active zone size, expressed as fraction of the size corresponding to the 101 node array simulation. As shown there, the projected amount of damage decreases, nearly linearly, with decreasing activation zone size. The red dashed lines represent a linear approximation of the resulted data points for all the cases, extrapolated to activation zone size equals zero. It is noted that the Base Case-NR calculations for the 101 node array simulation (fraction = 1 in the horizontal axis) is the same case for which the results were depicted for $\beta = 0.4 \text{ V}$ in Figure 2.

When local resistance was not taken into account (NR cases), the decrease of the damage projection with activation zone size was, for both variations of resistivity and oxygen diffusivity, toward nearly zero values for a terminally small node separation. The linear trend fit indicated $\sim 0.4 \%$ and -0.04% for the Base Case-NR and the Low DO_2 and ρ -NR cases respectively. In contrast, introduction of plausible R_s values by the procedure indicated earlier resulted in finite limit damage projections for the terminally small node separation. The linear limits in those cases were 6.4% and 2.0% for the Base Case-R and the Low DO_2 and ρ -R cases respectively.

Figure 10 displays the same results in log-log format and provide additional insight on the overall trends. Ignoring the presence of R_S results in trend lines with a nearly unity slope in the log-log graph over the entire range tested. When those trends were alternatively fit to a power law dependence of damage on active zone size exponents of 0.93 and 1.02 were obtained for the Base Case-NR and the Low DO_2 and ρ -NR cases respectively, confirming the nearly linear tendency toward a zero limit with decreasing zone size. In this display, the trends for the cases incorporating R_s show as curves that, given the linear trend toward finite limits in Figure 9, tend toward horizontal asymptotes corresponding to those limits.

The damage prediction at 60 years for the equivalent of the Base Case-NR (diamond) but assuming $\beta_{CT} = \infty$ is shown in Figure, describing a system with a threshold invariant with potential. The dashed line represents a linear approximation showing a result, ~31% damage that is much greater than for the other cases and also essentially independent of the activation zone size. This independence is to be expected since in the absence of TDP each node in the column acts independently of the others so the result should be the same regardless of the choice of fineness of the segment sizes used. The result serves also as a positive check of the robustness of the calculation procedures. It is noted that the system is the same for which the $\beta_{CT} = \infty$ results are given in Figure 1. It is noted also that the relative damage level results for the various cases also met the expectation, noted earlier, that in Low DO_2 and ρ conditions the damage should be less since the coupling effect between zones would be greater and the beneficial effect of TDP greater.

The results supports the validity of the hypothesis that as active zones become smaller their preventive throwing power would be reduced as well, resulting in the development of more numerous active zones that would make up for their individual smaller size in reaching to a finite damage terminal condition. Introducing the resistance polarization effect of R_S , resulted in a more realistic simulation of the extent to which a corroding zone prevents corrosion initiation in the surrounding regions. Conversely, the previous modeling approach projected unrealistically high prevention regions around existing corroding zones.

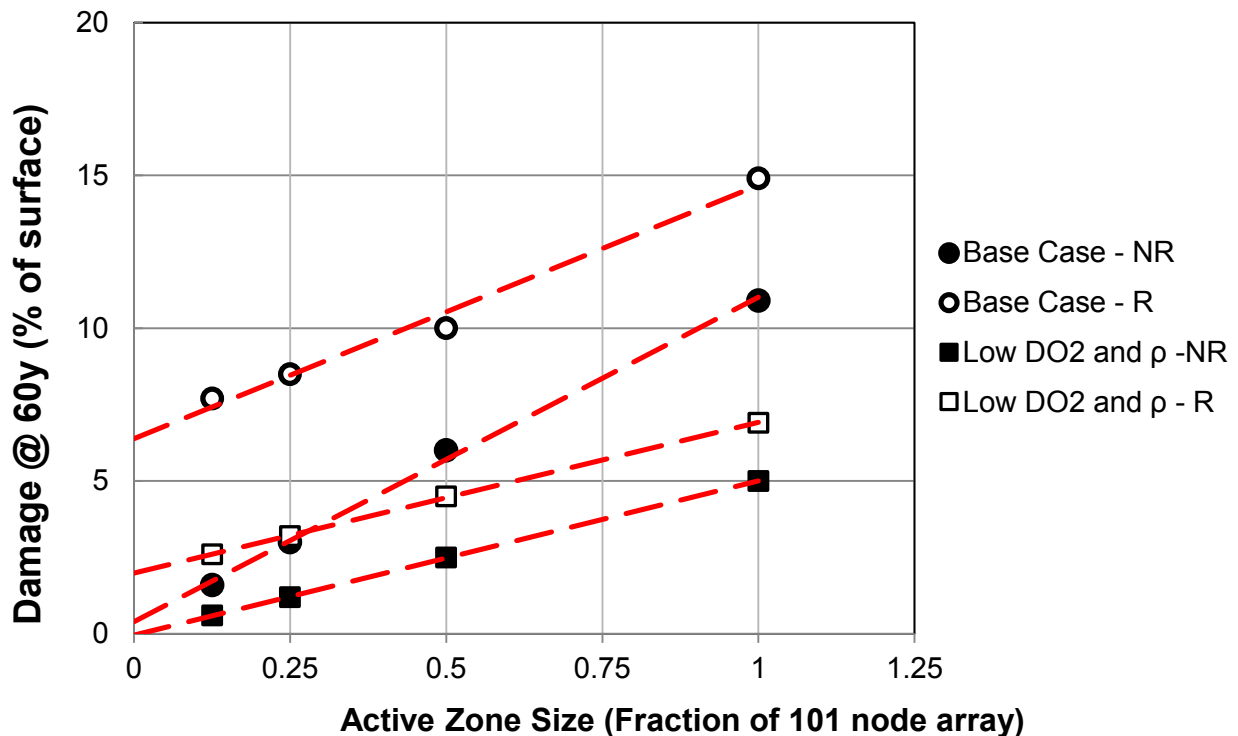


Figure 9. Damage forecast for year 60 as function of activation zone size.

©2013 by NACE International.

Requests for permission to publish this manuscript in any form, in part or in whole, must be in writing to NACE International, Publications Division, 1440 South Creek Drive, Houston, Texas 77084.

The material presented and the views expressed in this paper are solely those of the author(s) and are not necessarily endorsed by the Association.

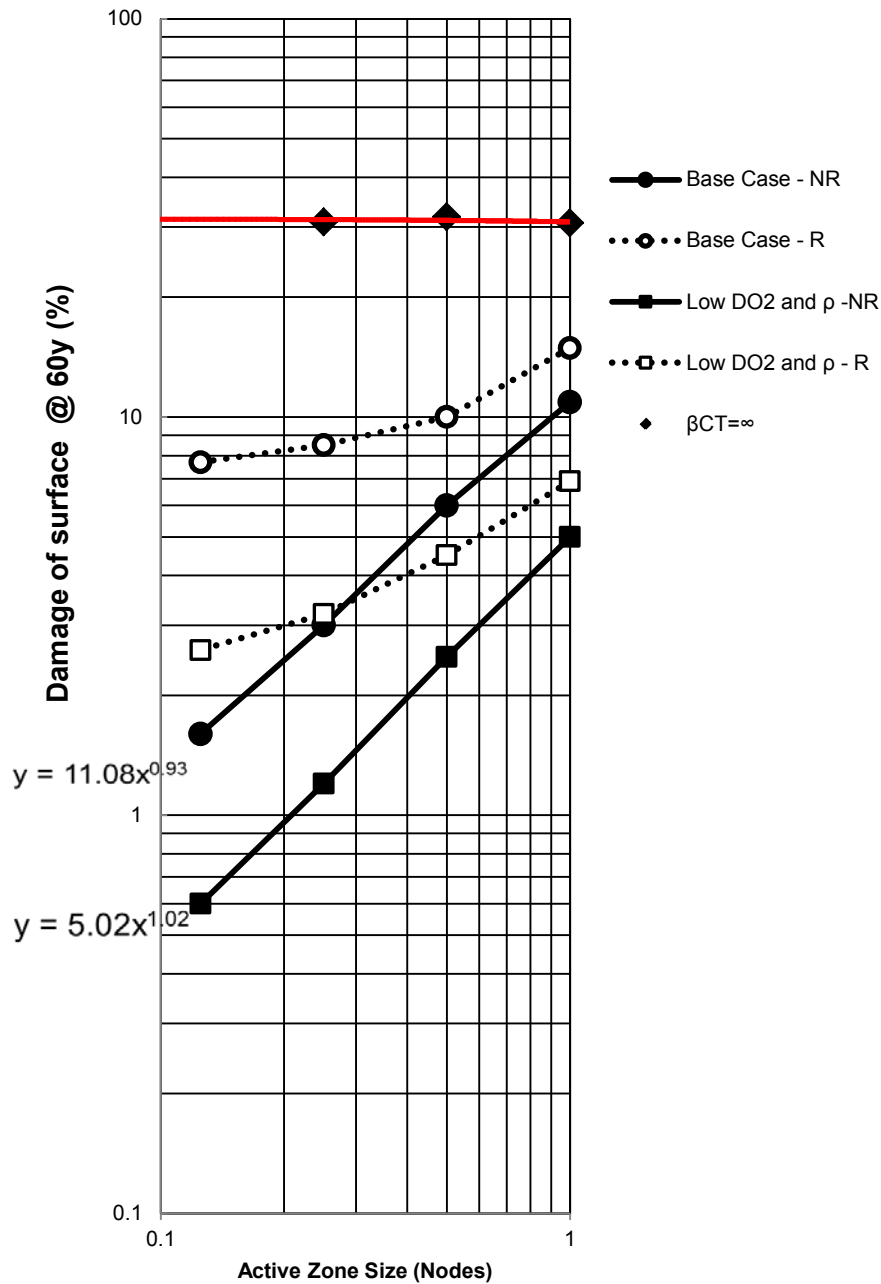


Figure 10. Damage forecast for year 60 as function of activation zone size. Dashed line represents the extrapolation of the system using β_{CT} .

CONCLUSIONS

- Exploratory calculations support the validity of the hypothesis that as active zones become smaller their preventive throwing power would be reduced as well, resulting in the development of more numerous active zones that would make up for their individual smaller size in reaching to a finite damage terminal condition.
- The model improvement over previous work stems from a more realistic implementation of the local concrete resistance R_S around the reinforcing steel bars.

ACKNOWLEDGEMENTS

This investigation was supported by the State of Florida Department of Transportation and the U.S. Department of Transportation. The findings and opinions presented here are those of the authors and not necessarily those of the supporting organizations.

REFERENCES

1. K. Tuutti, "Corrosion of Steel in Concrete" (ISSN 0346-6906), Swedish Cement and Concrete Research Institute, Stockholm, 1982.
2. A. N. Sánchez, A.A. Sagüés. "Chloride Threshold Dependence on Potential in Reinforced Mortar", NACE Corrosion 2012, Paper No. C2012-0001728, 11 pp., NACE International, Houston, 2012.
3. Alonso C., Castellote M., Andrade C. (2002) Chloride threshold dependence of pitting potential of reinforcements, *Electrochim. Acta*, 47, 3469-3481
4. F.J. Presuel-Moreno, A.A. Sagüés, S.C. Kranc. (2005). Steel Activation in Concrete Following Interruption of Long-Term Cathodic Polarization. *Corrosion*, Vol. 61, issue 5, pp. 428-436.
5. Kranc, S. C., & Sagüés, A. A. (2005). Cathodic Prevention Distribution in Partially Submerged Reinforced Concrete, (June), 548–558.
6. Pedferri, P., *Cathodic protection and cathodic prevention*. Construction and Building Materials, 1996. **10**(5): p. 391-402.
7. J. Bockris and K.N. Amulya. *Modern Electrochemistry 1: Vol. 1*. 2nd Edition. Plenum Press, New York. 1998.
8. A. A. Sagüés, S.C. Kranc, and K. Lau. "Service Life Forecasting for Reinforced Concrete Incorporating Potential-Dependent Chloride Threshold", NACE Corrosion 2009, Paper No. 09213, 22 pp., NACE International, Houston, 2009.
9. A. A. Sagüés, S.C. Kranc, and K. Lau. "Modeling Corrosion of Steel in Concrete with Potential-Dependent Chloride Threshold", 17th International Corrosion Congress, Paper No. 4006, 16 pp., NACE International, Houston, 2009.
10. "A.A. Sagüés and S.C. Kranc, Model for a Quantitative Corrosion Damage Function for Reinforced Concrete Marine Substructure", in *Rehabilitation of Corrosion Damaged Infrastructure*, p.268, Proc., Symp. 3, 3rd. NACE Latin-American Region Corrosion Congress, P.Castro, O.Troconis and C. Andrade, Eds., ISBN 970-92095-0-7, NACE International, Houston, 1998.
11. F. J. Presuel-Moreno, Kranc, S. C., & Sagüés, A. A. (2005). Cathodic Prevention Distribution in Partially Submerged Reinforced Concrete, , Vol. 61, p.548, 2005
12. H. Kaesche, *Metallic Corrosion*. NACE, Houston. 1996.
13. Kranc, S.C. and Sagüés, A.A. "Computation of Reinforcing Steel Corrosion Distribution in Concrete Marine Bridge Substructures", *Corrosion*, Vol. 50, p. 50, (1994)
14. S. C. Kranc and A. A. Sagüés. "Computation of Corrosion Macrocell Current Distribution and Electrochemical Impedance of Reinforcing Steel In Concrete", ASTM STP 1154, *Computer Modeling in Corrosion*, R. Munn, Ed., p. 95, American Society for Testing and Materials, Philadelphia, 1992.